8th International Symposium on Magnetic Bearing
August 26-28, 2002, Mito, Japan

OPTIMAL DESIGN OF PERMANENT MAGNET BEARINGS WITH APPLICATION TO THE HEARTQUEST™ VENTRICULAR ASSIST DEVICE

Chen Chen, Brad Paden

Magnetic Moments LLC, Santa Barbara, CA 93111, USA, chen@mmsb.com

James Antaki

Antakamatics Inc., Pittsburgh, PA 15213, USA

Jed Ludlow, Gill Bearnson

MedQuest® Products Inc., Salt Lake City, UT 84103

KEYWORDS

Magnetic Bearings, Design Optimization, Artificial Hearts

ABSTRACT

Closed-form design equations for magnetic bearings are desirable for design optimization of sophisticated electrical mechanical systems such as artificial hearts. We develop asymptotic approximations to force and stiffness characteristics of magnetic bearings formed from concentric permanent magnet rings having rectangular cross sections. The equations are well adapted to spreadsheets and facilitate an efficient numerical optimization process. The method was applied to the development of the HeartQuest™ VAD (ventricular assist device), which achieved remarkable compactness and stable operation.

INTRODUCTION

Design optimization is critical to the success of medical applications of magnetic bearing technology as there are typically competing performance objectives relating to force, stiffness, size and weight. Moreover, it is common in design practice that magnetic bearings compete for space with the other components in a system, and this competition is naturally formulated and resolved using the language and tools of optimization. In many cases, a magnetic bearing solution would only be possible when the system engineer had the freedom to design the entire system with trade-offs in mind.

Commercial finite element analysis (FEA) packages have greatly facilitated the conventional trial and error designing process. However, such a process breaks down in the case of complex and novel topology, where the geometry itself is a design variable. In addition, even the contemporary FEA products equipped with optimization algorithms are limited in the number of design variables subject to optimization. In order to achieve an optimal design, designers have to understand design relationships, trade-offs, and sensitivities of design changes. These demands explain the allure of analytical solutions and closed form equations that are suitable for rapid evaluation..

Within the scope of magnetic bearings formed from permanent magnets, the existing analytical methods come with various complexity and approximation [1-10]. The Backers' theory [1] represents a simple solution to stacks of alternately magnetized magnet rings that extend infinitely in the axial direction. Similar assumptions were used by Halbach who proposed the magnetic structure known as the Halbach array [2]. Despite of the usefulness of these approximations, a practical magnetic bearing may not be accurately modeled using infinite array approximations. Yonnet's model [3], on the other hand, deals with a single pair of magnets. However, the theory was based on the magnetic dipole model and is thus limited to magnets with sectional dimensions smaller than the air gap length. Many practical magnetic bearings do not fall into this category. Another set of closed-form equations utilized by Yonnet [4] removed such limitation on the size, but it has yet to be further developed to treat stacks of magnets with varying sizes or having a Halbach array structure. Another work in the area is typified by the development of a perturbative approach [5] to improve accuracy of bearing stiffness calculation for small diameter magnetic rings, which has to be used together with FEA. The model proposed by Furlani [6] is based

on dividing a magnet into small pieces and summing up forces between those pieces. It was considered unsuitable for our design needs in terms of the complexity in evaluating the expressions.

One may have noticed that various analytical solutions commonly stem from the basic principles of electromagnetism, which can be found in textbooks like Barger and Olsson [11] and Jackson [12]. Similarly, we started from the basic principles and developed a set of closed-form equations and corresponding methods to compute forces and stiffnesses of magnetic bearings. These met with our goal of having simple and accurate expressions for design optimization.

FRAMEWORK

We consider a magnetic bearing formed from a rigid magnet material, such as Neodymium-Iron-Boron (NdFeB), working in the range of constant magnetization. The magnetic bearing is formed from concentric magnet rings of rectangular cross-section, and we assume a uniform magnet material for each ring. This allows an axisymmetric model of the bearing. There is no limitation to the number of magnets involved.

A permanent magnet can be modeled with magnetization currents, which reduce to current sheets on the magnet surfaces if the interior magnetization is uniform [11,12]. Figure 1 shows two types of magnet rings under consideration, magnetized in axial or radial direction as indicated by the arrows. The bold sides of the cross-section indicate current sheets where the direction of current flow is given by the right-hand rule and the direction of magnetization. The models we are using are linear, so the magnetic forces in a sophisticated suspension can be obtained by simply summing up forces between each pair of magnets on the two bearing races. Figure 1 lists the four basic combinations of such elementary pairs, with the upper and lower rings belonging to different bearing races.

The current sheet model and the superposition principle enable us to compute the magnetic forces between two magnets by summing up the magnetic forces between their equivalent current sheets. Thus, the basic force calculation involves the interaction of two current sheets.

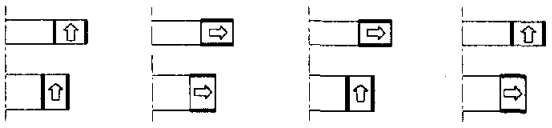

Figure 1 Basic combinations of magnet rings in a bearing unit and their equivalent current sheets (dashed line is axis of symmetry; only half section is shown)

Note that each elementary pair of magnet rings in Figure 1 consists of four combinations of current sheet pairs. In order to derive a general equation for all these combinations, we constitute a pair of L-shaped current sheets as shown in Figure 2. It is obvious that any of the current sheets in Figure 1 can be derived by assigning zero length to one leg of the "L". Therefore, equations for the force and stiffness between these L-shaped current sheets apply to any pair of interactive current sheets in our magnetic bearing models.

Figure 2 also indicates the geometric quantities defining the current sheet pair. In order to distinguish the race that exerts force from the race that experiences the force, a prime is used to symbol any of the quantities for the former race. A further convention is made that the joint of the two current sheets experiencing forces forms a corner to the lower left, and the joint of the two current sheets exerting forces forms a cornet to the upper right. Accordingly, the radial and axial distances between the two corners are

$$\Delta r = r - r' \tag{1a}$$

$$\Delta z = z - z' \tag{1b}$$

which may be positive, zero, or negative.

In order to calculate forces between concentric magnet rings in a cylindrical coordinates system (r, z), we start with a planar 2-D problem in (x, y), which is characterized by flat infinitely long current sheets, and then extend the results to the actual ring-shaped magnets. The coordinates x and y will correspond to the coordinates r and z respectively, and the same L-shaped current sheets as indicated in Figure 2 are used as the cross section in the planar 2-D model. Applying the classical solution to the magnetic force between two infinitely long current-carrying wires ([11], section 5-3) yields the following equations for the x and y components of the force on the upper right sheets in Figure 2.

$$f_x = \frac{\mu_0 H_C^2}{2\pi}\left\{\begin{matrix} U_1(W_z', W_z, \Delta r, \Delta z) + V_1(W_r', W_r, \Delta z, \Delta r) \\ + U_2(W_z', W_r, \Delta r, \Delta z) + U_2(W_z, W_r', \Delta r, \Delta z) \end{matrix}\right\} \tag{2}$$

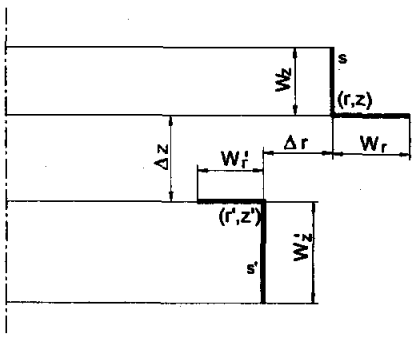

Figure 2 A pair of L-shaped current sheets for analysis

$$f_y = \frac{\mu_0 H_C^2}{2\pi}\begin{Bmatrix} V_1(W_z', W_z, \Delta r, \Delta z) + U_1(W_r', W_r, \Delta z, \Delta r) \\ + U_2(W_r', W_z, \Delta z, \Delta r) + U_2(W_r, W_z', \Delta z, \Delta r) \end{Bmatrix} \quad (3)$$

where μ_0 is the permeability of a vacuum (and air for practical purposes), H_c is the coercivity and the surface current density in the current sheet model, and

$$\begin{aligned} &U_1(w_1, w_2, \Delta_1, \Delta_2) \\ &= \frac{1}{2}\Delta_1 \ln\left\{\left(\Delta_1^2 + \Delta_2^2\right)\left[\Delta_1^2 + (w_1 + w_2 + \Delta_2)^2\right]\right\} \\ &- \frac{1}{2}\Delta_1 \ln\left\{\left[\Delta_1^2 + (w_2 + \Delta_2)^2\right]\left[\Delta_1^2 + (w_1 + \Delta_2)^2\right]\right\} \\ &+ (w_1 + \Delta_2)\tan^{-1}\frac{w_1 + \Delta_2}{\Delta_1} + (w_2 + \Delta_2)\tan^{-1}\frac{w_2 + \Delta_2}{\Delta_1} \\ &- (w_1 + w_2 + \Delta_2)\tan^{-1}\frac{w_1 + w_2 + \Delta_2}{\Delta_1} - \Delta_2 \tan^{-1}\frac{\Delta_2}{\Delta_1} \end{aligned} \quad (4)$$

$$\begin{aligned} &U_2(w_1, w_2, \Delta_1, \Delta_2) \\ &= \frac{1}{2}(w_1 + \Delta_2)\begin{Bmatrix} \ln\left[\Delta_1^2 + (w_1 + \Delta_2)^2\right] \\ - \ln\left[(w_2 + \Delta_1)^2 + (w_1 + \Delta_2)^2\right] \end{Bmatrix} \\ &+ \frac{1}{2}\Delta_2\left\{\ln\left[\Delta_2^2 + (w_2 + \Delta_1)^2\right] - \ln\left[\Delta_1^2 + \Delta_2^2\right]\right\} \\ &+ (w_2 + \Delta_1)\left[\tan^{-1}\frac{\Delta_2}{w_2 + \Delta_1} - \tan^{-1}\frac{w_1 + \Delta_2}{w_2 + \Delta_1}\right] \\ &- \Delta_1\left[\tan^{-1}\frac{\Delta_2}{\Delta_1} - \tan^{-1}\frac{w_1 + \Delta_2}{\Delta_1}\right] \end{aligned} \quad (5)$$

$$\begin{aligned} &V_1(w_1, w_2, \Delta_1, \Delta_2) \\ &= \frac{1}{2}(w_1 + \Delta_2)\ln\left[\Delta_1^2 + (w_1 + \Delta_2)^2\right] \\ &+ \frac{1}{2}(w_2 + \Delta_2)\ln\left[\Delta_1^2 + (w_2 + \Delta_2)^2\right] \\ &- \frac{1}{2}(w_1 + w_2 + \Delta_2)\ln\left[\Delta_1^2 + (w_1 + w_2 + \Delta_2)^2\right] \\ &- \frac{1}{2}\Delta_2 \ln\left[\Delta_1^2 + \Delta_2^2\right] \\ &+ \Delta_1\left[\tan^{-1}\frac{w_1 + \Delta_2}{\Delta_1} + \tan^{-1}\frac{w_2 + \Delta_2}{\Delta_1}\right] \\ &- \Delta_1\left[\tan^{-1}\frac{w_1 + w_2 + \Delta_2}{\Delta_1} + \tan^{-1}\frac{\Delta_2}{\Delta_1}\right] \end{aligned} \quad (6)$$

The extension of planer 2-D results to the axisymmetric situation follows methods employed in other investigations [1,3,4]. This results in a net zero radial force (due to concentricity). The net axial force is approximated by the planar 2-D force per unit depth multiplied by the average perimeter of the current sheet pair.

The average perimeter for the L-shaped current sheet pair is taken as the arithmetic average of the sheet legs.

$$R_{aver} = \frac{1}{2}(r + r') + \frac{1}{4}(W_r - W_r') \quad (7)$$

Therefore, the net axial force on the current sheet is:

$$F_z = \mu_0 H_C^2 R_{aver}\begin{bmatrix} V_1(W_z', W_z, \Delta r, \Delta z) + U_1(W_r', W_r, \Delta z, \Delta r) \\ + U_2(W_r', W_z, \Delta r, \Delta z) + U_2(W_r, W_z', \Delta r, \Delta z) \end{bmatrix} \quad (8)$$

Consider next the stiffness of the suspension. The axial stiffness in the L-shaped current sheet pair is obtained by partial differentiation of F_z with respect to Δz:

$$\begin{aligned} k_z &= -\frac{\partial F_z}{\partial \Delta z} \\ &= \mu_0 H_C^2 R_{aver}\begin{Bmatrix} S_1(W_z', W_z, \Delta r, \Delta z) - S_1(W_r', W_r, \Delta z, \Delta r) \\ - S_2(W_r, W_z', \Delta z, \Delta r) - S_2(W_r', W_z, \Delta z, \Delta r) \end{Bmatrix} \end{aligned} \quad (9)$$

with

$$\begin{aligned} &S_1(w_1, w_2, \Delta_1, \Delta_2) = \frac{1}{2}\ln\left\{\left(\Delta_1^2 + \Delta_2^2\right)\left[\Delta_1^2 + (w_1 + w_2 + \Delta_2)^2\right]\right\} \\ &- \frac{1}{2}\ln\left\{\left[\Delta_1^2 + (w_2 + \Delta_2)^2\right]\left[\Delta_1^2 + (w_1 + \Delta_2)^2\right]\right\} \end{aligned} \quad (10)$$

$$\begin{aligned} S_2(w_1, w_2, \Delta_1, \Delta_2) &= \tan^{-1}\frac{\Delta_2}{w_2 + \Delta_1} + \tan^{-1}\frac{w_1 + \Delta_2}{\Delta_1} \\ &- \tan^{-1}\frac{w_1 + \Delta_2}{w_2 + \Delta_1} - \tan^{-1}\frac{\Delta_2}{\Delta_1} \end{aligned} \quad (11)$$

The radial stiffness is obtained through application of the Earnshaw's theorem [3,4], which implies that the radial stiffness is half of the axial stiffness in an axisymmetric construction. That is,

$$k_r = -\frac{k_z}{2} \quad (12)$$

Finally, the angular stiffness with respect to axis r (normal to the z axial and passing through the origin) is obtained as:

$$k_\varphi = \left[-R_{aver}^2 + \left(z + W_z/2\right)^2\right]k_r \quad (13)$$

where z is the axial coordinate of the corner of the current sheets that experience force (Figure 2). It should be noted that the coordinate system is placed in such a way that the origin coincides with the bearing center. The bearing center is the point about which an infinitesimal rotation of the bearing component would not induce any bearing force of the same or higher order of magnitude. The bearing center can be found by computing moments of every current sheet comprising the whole suspension.

In summary, the following procedure can be followed to calculate the forces and stiffnesses in a magnetic bearing unit: First, replace the magnet rings with equivalent current sheets. Second, compute magnetic force and stiffness components between each pair of current sheets with the above equations. Finally, sum up all the interactive forces and stiffnesses to get the net force and stiffness of the bearing unit.

OPTIMAL DESIGN METHOD

The above equations conveniently fit into spreadsheets. For a bearing composed of m current sheets in one race and n current sheets in the other race, there are $m \times n$ elementary interactive forces/stiffnesses to be calculated. This corresponds to a matrix of $m \times n$ elements in a spreadsheet for each force or stiffness component (F_z, k_z, k_ϕ). Behind each element is an equation, and a summation of these elements' values gives the force/stiffness of the entire magnetic bearing.

Once the spreadsheet is constructed, the various numerical optimization algorithms can be applied. An optimal design should start with an analysis of all the relevant variables, so that the derived variables are distinguished from the design variables. (Design variables are those that all together define a particular design, and derived variables are calculated from the design variables and reflect the functions of the design.) Some of the design variables are to be optimized, such as the magnet dimensions; the others are already specified, such as the air gap length. In the set of the derived variables, one variable such as the stiffness is chosen as the objective, or cost function, that is to be minimized or maximized. In addition, there are a set of constraints to define the limits for certain design variables or derived variables based on interactions with other components in the system design. In many cases, a variable can be either treated as an objective or grouped into the constraints set, depending on the design approach.

Optimization on a sophisticated system consisting of more components may follow an interactive designing process wherein constraints are negotiated among subsystem designers. Each of the subsystems is to be optimized subject to constraints from the other subsystems, and the design iteration has to end up with optimization at the system level.

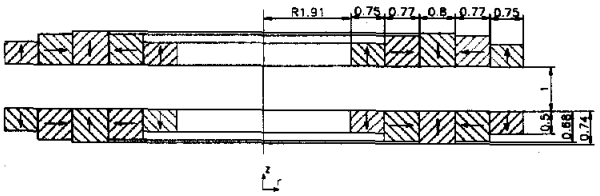

Figure 3 An design example of optimized Hallbach type magnetic bearing

The stated magnetic bearing design method has demonstrated remarkable effectiveness and productivity in our design practice. As an example, Figure 3 is an optimized Halbach type magnetic bearing composed of ten magnetic rings. All dimensions of the magnets were determined by the optimization "solver" in Microsoft Excel with the objective of maximizing the stiffness per unit cross sectional area of the magnet array (including all magnets). The generalized reduced gradient (GRG2) nonlinear optimization solver embedded in Microsoft Excel was used and demonstrated rapid and robust convergence for this type of problem. The dimensions shown in Figure 3 are relative to the air gap length, and the inner radius of the bearing was pre-set to be 1.91. All the magnets are the same material. A FEA was performed to calculate the force and stiffness of that bearing. The differences between our closed-form expressions and the FEA were roughly 3%.

APPLICATION TO THE HEARTQUEST™ VAD DESIGN

The HeartQuest™ ventricular assist device (VAD) is a magnetically levitated centrifugal pump designed for left-ventricular assistance. The design philosophy of the HeartQuest™ VAD is to achieve system optimization by means of the application of mathematical modeling and optimization. The pump is divided into subsystems including passive (permanent magnet) suspension, active suspension (voice coil actuator), electric motor, mean line flow, and clearance flow. Closed-form design equations were developed for each of the subsystems. In addition, rigid-body rotordynamic analysis was performed to ensure stability of the suspension.

With the aid of the spreadsheets, more than a dozen design concepts (topologies) were quickly optimized and evaluated. Figure 4 depicts the chosen topology, where the rotor contains an annular hub supporting the impeller blades, and the stator (or housing) involves a central spindle, a bottom, and an outer peripheral

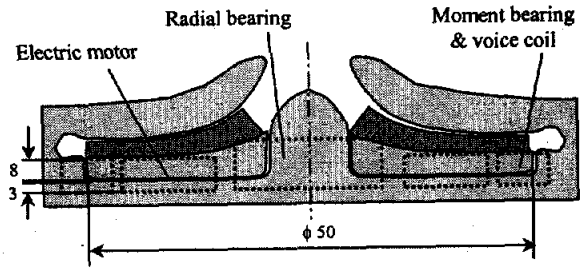

Figure 4 Schematic cross sectional view of the HeartQuest™ VAD showing the magnetic bearing configuration

construction that surround the rotor hub. The hub accommodates all suspension and motor components in the rotor. Permanent magnet bearings are implemented in the inner bearing to provide positive radial stiffness, as well as in the outer bearing to provide positive tilting stiffness. The magnets in the outer bearing also serve as magnets for a linear actuator referred to as the "voice coil" to provide active control in the axial direction.

Of particular importance in the design of such magnetic bearing system is the accuracy of the force and stiffness calculation. According to Earnshaw's theorem and the relationship (13), the outer bearing contributes a negative radial stiffness ($k_{r2}<0$) and a positive tilting stiffness ($k_{\phi 2}>0$); the inner bearing, depending on its aspect ratio, may induce a negative titling stiffness ($k_{\phi 1}<0$, possibly) although it offers a positive radial stiffness ($k_{r1}>0$). The net radial or tilting stiffness is the difference between the two stiffnesses: $k_r = k_{r1} + k_{r2}$, and $k_\varphi = k_{\varphi 1} + k_{\varphi 2}$. The radius of the outer bearing, R_{aver2}, is limited by pump size. Hence, to meet the required tilting stiffness, there is a lower limit on the absolute value of the negative radial stiffness in the outer bearing, k_{r2}. The radial stiffness in the inner bearing, k_{r1}, must be more than this to cancel the negative stiffness of the outer bearing. However, the former is limited by the allowable space for the inner bearing unit. These trade-offs led to a design where the two radial stiffnesses are of the same order of magnitude. In fact, the net stiffness is a relatively small number arrived at by the subtraction of two big numbers. Consequently, the fractional errors in force/stiffness of the individual bearing components are amplified in the fractional error in the net force/stiffness. It follows that the individual bearing stiffnesses must be carefully calculated and controlled in manufacturing.

The accuracy requirements were an issue with the FEA. When performing FEA, we checked the difference between the rotor and stator forces, which in theory should be equal in magnitude and opposite in sign but varied significantly with the coarseness of the FEA grid and the computational method. We set a 5%

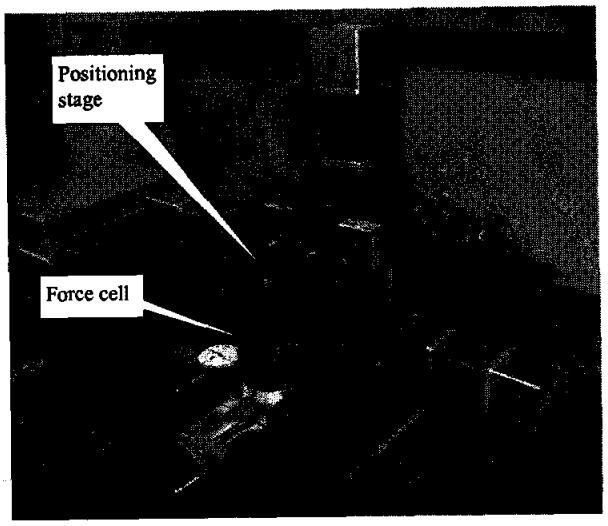

Figure 5 The stiffness test fixture, showing the positioning stage and the force cell

limit for the allowed force difference relative to the force we used to calculate the stiffness through differentiation. Three dimensional FEA was performed using Ansoft. We observed that the error limit had not been met until the number of the finite elements went beyond 200,000 and the computing time became unacceptable for practical optimal design process.

Nevertheless, the equations developed in this work exhibited satisfactory accuracy to meet the design purpose with negligible computing time. In a period of several months, more than one hundred detailed designs were produced and evaluated. This led to an impeller hub only 8 mm thick with 50 mm outer diameter. The corresponding bearing and electric motor components on the housing occupy a 3 mm thick space on the bottom (Figure 4). The suspension achieved more than a 40% margin relative to the first critical speed for both transverse and precession rotor resonance. It also possessed sufficient stiffnesses to reject external disturbances including fluid loads and housing shock.

The HeartQuest prototypes have experienced force and stiffness verification tests for the assembled as well as the individual magnetic bearing components. Figure 5 shows a custom-built test fixture, which consists of a positioning stage that moves the rotor component to desired positions and a stationary force cell that holds the stator component to measure its force and torque components (the rotor and stator are not shown in the Figure). The stage produces radial, axial, and angular (titling) displacements at an accuracy within 2.54 micron for the linear positioning, and within 0.0001 rad for the angular positioning. The force cell is a 6 degree-of-freedom force and torque sensor with accuracy of 0.025 Nt for forces and 0.5 Nt-mm for torques measurements.

In addition to force testing, magnets are subjected to magnetic property tests prior to assembly. These include measurements of the remanence flux density (Br) based on the Helmholtz coils technique. Although the manufacturer specified Br was used for the optimal design, the measured Br was used as substitution in the force/stiffness calculation to check against the experiments.

Satisfactory accuracy of the spreadsheet has been verified. Typical tests on the inner or outer bearing components resulted in less than 7% error between the measured and predicted stiffnesses when the bearings did not involve any ferromagnetic material. Note that the entire assembly of the real pump involves a small amount of iron that negatively influences the accuracy of the spreadsheet. However, FEA and experiments showed that that influence was small enough to be neglected in practice. For the various detailed designs that were tested, the difference between measured and predicted stiffness components was within 20% in most cases. This made it possible to introduce correction factors for the iron effects and eventually corrected the error for the engineering designs.

Besides the ferromagnetic effects, the imperfections in magnet material and mechanical tolerances are the other major contributors to the errors mentioned above. Those sources of error are difficult to model even with FEA. The present theory and optimization method provided a powerful tool for rapid design of magnetically levitated artificial hearts.

DISCUSSION

The present theory is limited to systems where the 2D model is applicable. This requires concentric magnet rings, as well as large bearing radius relative to the air gap length of the bearing. The latter has not been a problem in our designs, however.

In general, the theory does not apply to systems with soft ferromagnetic material involved. Although highly permeable material can be treated as a mirror for permanent magnet images in some instances, such treatment goes beyond the scope of this paper. The theory's successful application in the HeartQuest product was based on the fact that the design process has justified a topology of a virtually iron free magnetic bearing, and ferromagnetic materials in the other part of the pump have minor influence on the suspension. When a system includes ferromagnetic material or soft permanent magnets (e.g. Alnico), the applicability of the present theory would have to be verified through FEA. In fact, a design process using FEA to correct closed form equations may take advantage of both approaches.

Since the force and stiffness both vary with the squared coercive force of the magnets, it is important for the design calculation to use magnetic properties as close to the true values as possible. In addition, the non-uniformity of the material and mechanical misalignment of the magnetization direction all contribute to errors and must be taken into account in the design process.

REFERENCES

1. Backers, F.T., A magnetic journal bearing, Philips Tech Rev, 22:232-8, 1960/61.
2. Halbach, K., Application of permanent magnets in accelerators and electron storage rings, J Appl Phys, 57:3605-8, 1985.
3. Yonnet, J.P., Permanent magnet bearings and couplings, IEEE Trans Magn, 17:1169-73, 1981.
4. Yonnet, J.P., Analytical calculation of magnetic bearings, Proc 5th Intern Workshop Rare Earth-Cobalt Perm Mag and Their Appl, 199-216, 1981.
5. Marinescu, M. and Marinescu, N., A new improved method for computation of radial stiffness of permanent magnet bearings, IEEE Trans Magn, 30:3491-4, 1994.
6. Furlani, E.P., A formula for the levitation force between magnetic disks, IEEE Trans Magn, 29:4165-9, 1993.
7. Akoun, G. and Yonnet, J.P., 3D analytical calculation of the forces and exerted between two cuboidal magnets, IEEE Trans Magn, 20:1962-4, 1984.
8. Delamare, J., Yonnet, J.P., and Rulliere, E., A compact magnetic suspension with only one axis control, IEEE Trans Magn, 30:4746-8, 1994.
9. Antila, M.J., The load capacity and stiffness of the axial permanent magnet bearings, Proc 4th Intern symp Mag Bearings, 287-291, 1994.
10. Krist, P., Gerber, R., Boehm, J., et al. Ponderomotive interactions between arrays of permanently magnetized rectangular prisma, IEEE Trans Magn, 29:2935-2937, 1993.
11. Barger, V.D., Olsson M.G.. in Classical electricity and magnetism: A contemporary perspective, Allyn and Bacon Inc., 1987.
12. Jackson J.D., in Classical electrodynamics, 2nd ed., John Wiley & Sons, 1975.